AJNR

In Vivo High-Resolution MR Imaging of Neuropathologic Changes in the Injured Rat Spinal Cord

T. Weber, M. Vroemen, V. Behr, T. Neuberger, P. Jakob, A. Haase, G. Schuierer, U. Bogdahn, C. Faber and N. Weidner

AJNR Am J Neuroradiol 2006, 27 (3) 598-604
http://www.ajnr.org/content/27/3/598

ORIGINAL RESEARCH

In Vivo High-Resolution MR Imaging of Neuropathologic Changes in the Injured Rat Spinal Cord

T. Weber
M. Vroemen
V. Behr
T. Neuberger
P. Jakob
A. Haase
G. Schuierer
U. Bogdahn
C. Faber
N. Weidner

BACKGROUND AND PURPOSE: MR imaging is the most comprehensive noninvasive means to assess structural changes in injured central nervous system (CNS) tissue in humans over time. The few published in vivo MR imaging studies of spinal cord injury in rodent models by using field strengths ≤7T suffer from low spatial resolution, flow, and motion artifacts. The aim of this study was to assess the capacity of a 17.6T imaging system to detect pathologic changes occurring in a rat spinal cord contusion injury model ex vivo and in vivo.

METHODS: Seven adult female Fischer 344 rats received contusion injuries at thoracic level T10, which caused severe and reproducible lesions of the injured spinal cord parenchyma. Two to 58 days postinjury, high-resolution MR imaging was performed ex vivo (2) or in vivo in anesthetized rats (5 spinal cord injured + one intact control animal) by using 2D multisection spin- and gradient-echo imaging sequences, respectively, combined with electrocardiogram triggering and respiratory gating.

RESULTS: The acquired images provided excellent resolution and gray/white matter differentiation without significant artifacts. Signal intensity changes, which were detected with ex vivo and in vivo MR imaging following spinal cord injury, could be correlated with histologically defined structural changes such as edema, fibroglial scar, and hemorrhage.

CONCLUSIONS: These results demonstrate that MR imaging at 17.6T allows high-resolution structural analysis of spinal cord pathology after injury.

MR imaging represents a powerful means to noninvasively visualize pathomorphologic changes in humans following spinal cord injury.[1,2] MR imaging findings correlate with histopathologic sequelae observed after spinal cord injury such as edema, hemorrhage, and secondary degenerative changes such as cyst formation. Moreover, MR imaging enables prediction of the severity of neurologic deficits after spinal cord injury.[3] On an experimental level, regenerative strategies have been validated in animal models of spinal cord injury, which promote functional and structural recovery. In particular, cell-based transplantation strategies hold great promise in regenerating the injured spinal cord.[4-10] Ultrastructural restoration in animals is primarily assessed by postmortem microscopicic analysis of spinal cord parenchyma. To be able to monitor regenerative strategies in clinical applications, noninvasive imaging techniques are mandatory. Only animal studies allow direct correlation of in vivo MR imaging data with histologic postmortem data as a prerequisite for proper interpretation of MR imaging findings in human studies after therapeutic interventions. Anatomic structures that must be resolved in mice or rats are 5–10 times smaller than in humans. This implies that volume elements in imaging data are smaller by a factor of roughly 100–1000. MR imaging studies of the spinal cord of rodent models, widely used to assess the efficacy of regenerative strategies following spinal cord injury, require a sufficiently high signal intensity–to-noise ratio (SNR) to resolve small-scale structures with satisfactory contrast. Furthermore, respiratory motion and blood flow may induce image artifacts. Structural changes occurring after spinal cord injury such as edema, cystic defects, atrophy, and hemorrhage have been detected in several MR imaging–based in vivo studies[11–19]; however, partial volume effects resulting from a lower spatial resolution in these studies reduced the reliability to exactly allocate and interpret signal intensity changes seen with MR imaging. Furthermore, studies demonstrating an acceptable spatial resolution employed implantable coils, which, unlike surface coils, require an additional invasive procedure. In the present study, we investigated whether high-field MR imaging at 17.6T would provide superior spatial resolution and thus improved detection of structural changes in the adult rat spinal cord following a defined contusion injury ex vivo and in vivo.

Received May 2, 2005; accepted after revision July 26.

From the Department of Physics, EP5 (Biophysics), University of Würzburg (T.W., V.B., T.N., P.J., A.H., C.F.), Würzburg, Germany; Department of Neurology, University of Regensburg (T.W., M.V., U.B., N.W.) and Institute for Neuroradiology, Bezirksklinikum Regensburg (G.S.), Regensburg, Germany; and the Department of Urology, Technical University (M.V.), Munich, Germany.

T.W. and M.V. contributed equally to this study.

Presented in part at the annual meeting of the Society for Neuroscience, New Orleans, Louisiana, Nov. 8–12, 2003; the annual meeting of the Deutsche Gesellschaft für Medizinphysik, Heidelberg, Germany, Oct. 1–4, 2003; the 7th International Conference on Magnetic Resonance Microscopy, Salt Lake City, Utah, Sept. 21–26, 2003; and the International Society for Magnetic Resonance in Medicine, Kyoto, Japan, May 15–21, 2004.

Address correspondence to Norbert Weidner, MD, Department of Neurology, University of Regensburg, Universitaetsstrasse 84, 93053 Regensburg, Germany.

Methods

Animals

The spinal cord injury and imaging experiments were conducted by using 8 young adult female Fisher 344 rats weighing 160–180 g. Ex vivo MR imaging was performed in 2 spinal cord–injured animals and in vivo MR imaging in 5 spinal cord–injured (Table 1) and one uninjured rat. All experiments were carried out in accordance with the European Communities Council Directive (86/609/EEC) and institutional guidelines for animal care. All efforts were made to minimize the number of animals used, as well as their suffering.

Table 1: Time table of in vivo MR imaging (MRI) scans for each animal

Animal No.	First MRI Scan (Days Postinjury	Second MRI Scan (Days Postinjury)	Third MRI Scan (Days Postinjury)	Histology
1	18	25	39	No*
2	18	25	39‡	No*
3	6	38	58	No*
4	2	38	—	Yes†
5	2	13§	58‖	Yes†

*Animals died during or shortly after last MRI scan.
†Animals sacrified one day after the last MRI scan.
‡Illustrated in Fig 5.
§Illustrated in Fig 4*A–C*.
‖Illustrated in Fig 4*D–F*.

Surgical Procedures

For the surgical procedure animals underwent anesthesia made up of a mixture of ketamine (62.5 mg/kg body weight; WDT, Garbsen, Germany), xylazine (3.175 mg/kg body weight; WDT), and acepromazine (0.625 mg/kg body weight, Sanofi-Ceva, Düsseldorf, Germany) in 0.9% sterile saline solution. Rats received spinal cord contusion injuries by using the Infinite Horizon (IH) Impactor spinal cord injury device (Precision Systems & Instrumentation, Lexington, Ky) as described elsewhere.[20] A laminectomy was performed at T10 to expose the dorsal portion of the spinal cord. The animals were suspended by attaching Adson forceps to the rostral T9 and caudal T11 vertebral bodies. Particular care was taken to align the exposed spinal cord perpendicular to the axis of the Impactor. The 2.5-mm stainless steel impounder tip was lowered to approximately 3–4 mm above the surface of the exposed spinal cord. The contusion injury was finally induced by applying an impact force of 2 Newton (equal to 200 kilodyne) to the exposed spinal cord at a velocity of 130 mm/s. Overlying muscle layers were sutured and the skin was closed. Postoperatively, animals were kept warm, placed on beds of sawdust, and given manual bladder evacuation twice a day for a period of ≤10 days as necessary and received intramuscular injections of 10 mg Cotrimoxazol (Ratiopharm, Ulm, Germany) once daily for a period of 10 days. Animals regained automatic neurogenic bladder function after 5–10 days.

MR Scanner

All MR imaging experiments were conducted on a vertical Bruker 750 wide-bore magnet system (Bruker Biospin, Rheinstetten, Germany) at 17.6T with a bore size of 89 mm.

In Vivo MR Imaging

Anesthesia was induced by inhalation of 4% isoflurane and maintained with 2% isoflurane in carbogen (95% oxygen and 5% carbon dioxide). Body temperature was maintained by heating the gradient cooling unit to 37 ± 2°C.

A total of 5 rats underwent in vivo MR imaging between 2 and 58 days after thoracic spinal cord contusions were applied (Table 1). An uninjured rat with an intact spinal cord served as control. An animal gradient system with 57-mm inner diameter and 0.2 T/m was used. Because of space restrictions within the gradient system, imaging of the rat spinal cord by using wide-bore magnets was not possible with commercially available hardware. Therefore, a probe head and surface coil were custom built to provide maximum space for adult rats as described.[21] The surface coil was designed as a transmit-receive coil in a half-cylindrical carrier mounted on an optimized probe base. The probe base included balancing units (baluns), which are important at higher frequencies because of the increased sensitivity of the electrical setup to imbalances.

To avoid artifacts caused by blood flow and respiratory motion, a triggering unit (RAPID Biomedical, Würzburg, Germany) for combined electrocardiogram (ECG) triggering and respiratory gating was used.

A multisection 2D spoiled gradient-echo sequence was used with an echo time (TE) around 4 milliseconds, depending on the exact spatial resolution used, and a repetition time (TR) around 200 milliseconds depending on the heart rate. As many as 9 sections were acquired per scan. By using surface coils, gradient-echo sequences are advantageous for transmission, because they are far less sensitive to radio-frequency (RF) inhomogenities. Two interleaved multisection datasets were acquired to cover a full 3D volume. The spatial resolution was at least 78 × 78 μm in-plane with a section thickness of 370 μm in axial sections and 156 × 98 μm in-plane with a section thickness of 370 μm in sagittal sections. Each series took 15–20 minutes.

Ex Vivo MR Imaging

For ex vivo MR imaging, one animal was perfused at 2 weeks and another animal at 4 weeks after the contusion injury with 150 mL cold 0.1 mol/L phosphate buffered saline (PBS) followed by 400 mL 4% paraformaldehyde in PBS. Spinal cords were removed and postfixed overnight in 4% paraformaldehyde in PBS and then left for 1 day in PBS containing 30% sucrose at 4°C. This fixation procedure is required for the histologic evaluation following ex vivo MR imaging. For the actual imaging process, spinal cord specimens were transferred into 5-mm-wide NMR tubes (Wilmad, Buena, NJ) filled with PBS containing 30% sucrose. Air bubbles were removed from the tube by using a vacuum pump and leaving each sample at a pressure of approximately 50 millibars for around 10 minutes.

A gradient system with 1 T/m and an inner diameter of 40 mm was used with a commercial 5-mm linear birdcage resonator as transmit and receive coil. The sample was kept at 20 ± 1°C during imaging experiments.

Positioning of the sample was performed by using a 3D low-resolution gradient-echo sequence. A 2D multisection spin echo with a TE of 7.5 milliseconds, a TR of 2 seconds, 24 signal intensity averages (NA), and a total scan time 3.5 hours was used. With a field of view (FOV) of 6 × 6 mm and an acquisition matrix of 256 × 256, the spatial resolution was 23 × 23 μm in-plane with a section thickness of 300 μm. A total of 30 sections were acquired in axial direction and 14 sections in sagittal direction.

Histology

Animals were transcardially perfused with a 0.9% saline solution followed by 4% paraformaldehyde in PBS 2 days after the final in vivo MR imaging. The spinal cords were removed, postfixed overnight in 4% paraformaldehyde in PBS and left for 1 day in PBS containing 30% sucrose. Sagittal 35-μm-thick sections of the thoracic spinal cord containing the injured area were cut with a cryostat. Every seventh section was immediately mounted on glass slides for Nissl staining. In the remaining sections, Prussian-blue staining and light-level immunohistochemistry were performed for a more detailed morphologic analysis of the contused spinal cord tissue. Prussian-blue staining, which was employed to detect hemosiderin deposits, was performed as follows: sections mounted on gelatin-coated slides were immersed in a solution of 4% potassium ferrocyanide and 4% HCl for 15 minutes. After several rinses, sections were counterstained with Vector Nuclear Fast Red solution (Linaris, Wertheim, Germany) for 5 min-

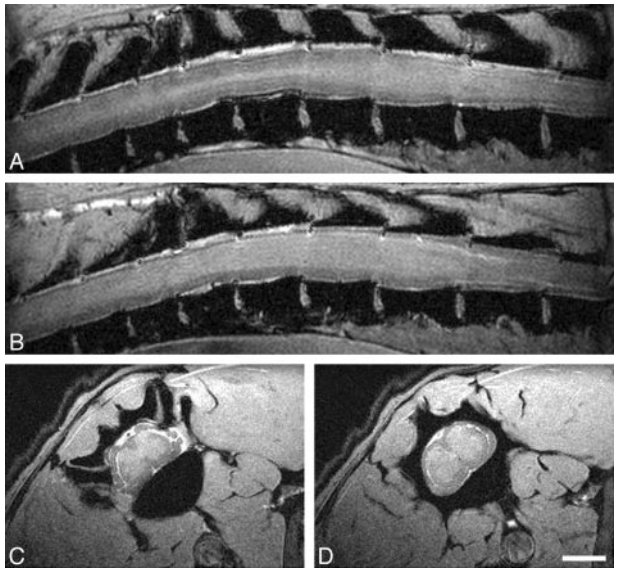

Fig 1. In vivo MR imaging of intact spinal cord at 17.6T. Panels *A* and *B* show sagittal scans through the thoracic spinal cord (section thickness, 239 μm; FOV, 40 × 30 mm; in-plane resolution, 156 × 117 μm; TR, ~200 milliseconds, depending on heart rate; TE, 4.4 milliseconds). Panels *C* and *D* display axial scans through the thoracic spinal cord (section thickness, 500 μm; FOV, 17.7 × 35.5 mm; in-plane resolution, 69 × 69 μm; TR and TE, as above). Scale bar, 2 mm. *A,* A more lateral sagittal scan depicts primarily white matter (lower signal intensity) with some longitudinally oriented more hyperintense structure, reflecting the gray matter of the lateral ventral horn. CSF appears hyperintense, vertebral bodies are hypointense. *B,* Most of the spinal cord parenchyma displayed here represents gray matter (hyperintense) surrounded by white matter tracts (hypointense) in a paramedian sagittal scan through the spinal cord. *C,* An axial scan through the thoracic spinal cord allows the clear distinction between the typical butterfly appearance of the spinal cord gray matter and the surrounding hypointense white matter. Also of note, spinal roots can be clearly identified at this level. *D,* A subsequent scan more caudally shows the spinal cord in cross-section away from the spinal root entry zone.

utes and dehydrated before coverslipping with Neo Mount (Merck, Darmstadt, Germany). For immunohistochemistry, the following primary antibodies were used: mouse-anti-GFAP (for astrogliosis; DAKO, Glostrup, Denmark; at 1/2000), goat-anti-collagen type III (for the fibrous scar; Southern Biotechnology, Birmingham, Ala, at 1/100) and mouse anti-rat monocytes/macrophages (clone ED1; Chemicon, Hofheim, Germany, at 1/1000). The sections were blocked in TBS + 3% donkey serum +0.1% Triton-X, and incubated with the primary antibody in tris-buffered saline (TBS) + 3% donkey serum +0.1% Triton-X overnight at 4°C on a rotating platform. The following day, sections were incubated with the secondary antibody (biotinylated donkey IgG; Jackson, Hamburg, Germany; at 1/1000) in TBS containing 3% donkey serum +0.1% Triton-X. Sections were incubated with avidin-biotinylated-peroxidase complex (Vector Elite kit; Linaris) followed by development for 3–15 minutes in a 0.05% solution of 3,3′-diaminobenzidine, 0.01% H_2O_2, and 0.04% nickel chloride in TBS yielding a brown-black reaction product. Sections were mounted onto gelatin-coated glass slides, air-dried, dehydrated, and coverslipped with Neo Mount (Merck). The histologic analysis was performed by using a Leica DMR microscope equipped with a Spot CCD camera model 2.2.1 (Diagnostic Instruments, Sterling Heights, Mich).

Results

In Vivo MR Imaging of Intact Spinal Cord

Gradient-echo MR imaging with ECG triggering and respiratory gating yielded high-resolution images of intact thoracic rat spinal cord in vivo without significant motion artifacts (Fig 1). The typical butterfly-shaped gray matter could be clearly distinguished from the less-intense surrounding white matter axonal tracts. The CSF surrounding the spinal cord appeared as a small hyperintense rim adjacent to the spinal cord due to its longer T2 and $T2^*$ relaxation times. With the applied sequence vertebral bodies appeared completely dark, whereas vertebral disks were bright.

Ex Vivo MR Imaging of Contused Spinal Cord

Spin-echo images of excised spinal cord 4 weeks after a thoracic contusion injury revealed a signal intensity pattern away from the injury epicenter in axial sections (Fig 2), which was almost identical to in vivo gradient-echo images in unlesioned animals (Fig 1*C, -D*). Gray matter was hyperintense compared with white matter. The central canal could be clearly identified. The gray/white matter differentiation completely vanished at the contusion center (Fig 2*G, -H*). The homogenous hyperintense signal intensity, which was pronounced in the spinal cord center and diminished toward the surface of the cord in all directions, was only interrupted by areas of signal intensity loss in the center of the cord, which were confined mostly to the gray matter (Fig 2*G*). Trauma-induced hemorrhage and consecutive hemosiderin deposits are the likely pathologic correlates for this signal intensity–free area, which have been described to occur frequently within the spinal cord gray matter after injury.[17] Hypointensities within the lesion center (in particular in sagittal MR images)—not as pronounced as the described hemosiderin-associated changes—corresponded to immunoreactivity for collagen type III, but not GFAP, in sagittal histologic sections (Fig 3*B, -J, -N*), thus representing components of the fibrous rather than the gliotic scar. The overall diameter of the cord was reduced. In particular the dorsolateral columns were symmetrically diminished in volume (Fig 2*G, -H*), reflecting substantial irreversible atrophy as soon as 4 weeks after injury. In some Nissl-stained sections (Fig 3*G*) all types of organized tissue were absent, which suggests a developing fluid-filled cavity; however, corresponding MR imaging scans did not display a homogenous hyperintensity (Fig 3*C*), which would be the MR equivalent of a cystic lesion defect. Instead, only a small hyperintense band—the correlate of the true cystic lesion defect—surrounded a hypointense core. Thus, it is likely that this hypointense area contained nonorganized material (inflammatory cells and cell debris mixed with hemosiderin deposits), which is regularly lost during the process of histologic analysis.

Remote from the lesion center, some neuroanatomically restricted signal intensity changes could be observed (Fig 2*A, -J–L;* Fig 3*B*). Hypointensities strictly confined to either the former main dorsal corticospinal tract caudal to the lesion or the ascending proprioceptive pathways (gracile fascicle) rostral to the lesion were identified. Hyperintense regions within the dorsal columns rostrally and caudally (Fig 2*B–D, -J–L;* Fig 3*A, -B*) can be attributed to cystic necrotic zones, which were identified in the corresponding sagittal histologic sections (Fig 3*F*). There was no difference in overall signal intensity changes compared with the spinal cord sample, which was taken 2 weeks after the contusion injury (data not shown).

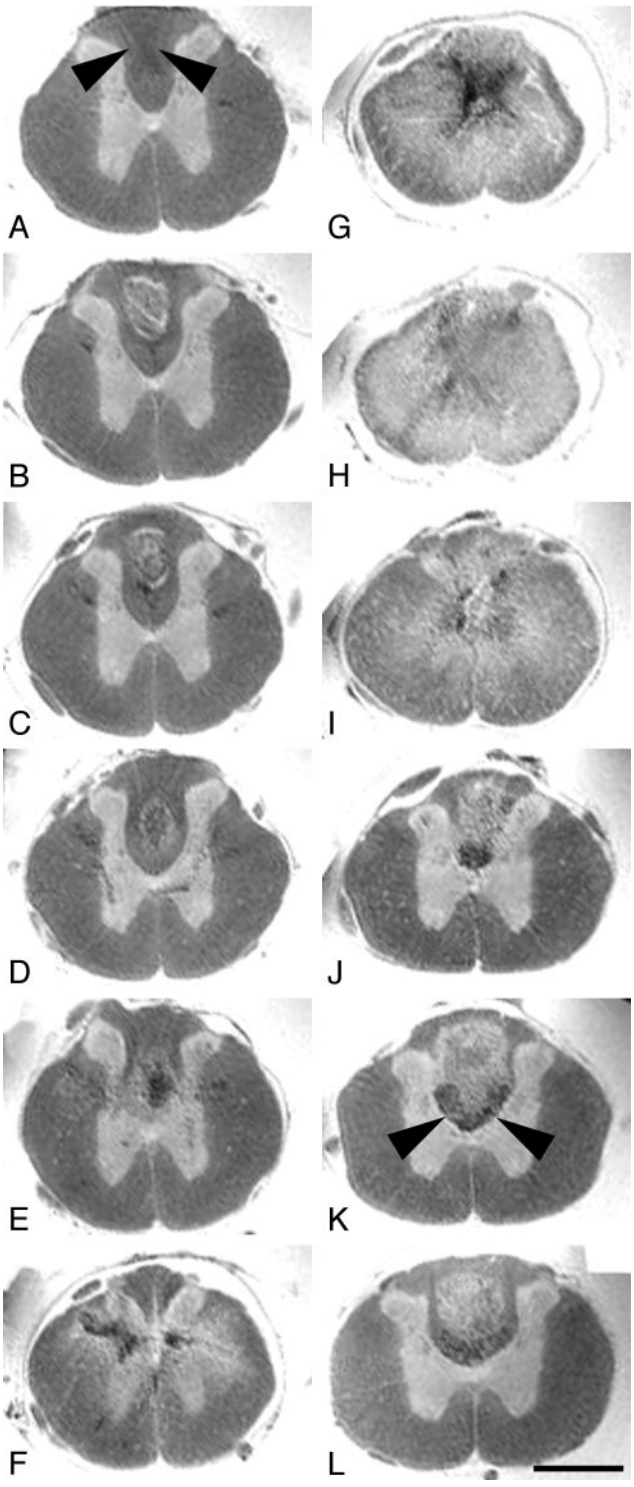

Fig 2. Axial ex vivo MR imaging scans of contused rat spinal cord. Axial sections of ex vivo MR imaging show microscopy grade visualization of morphologic changes in the injured rat spinal cord 4 weeks after contusion injury at midthoracic level (2D multisection spin-echo; section thickness, 300 μm; FOV, 6 × 6 mm; in-plane resolution, 23 × 23 μm; TE, 7.5 milliseconds; TR, 2 seconds). Scale bar, 1 mm. Panels *A–L* show consecutive sections in the rostral-caudal direction. In rats the dorsal columns contain not only ascending proprioceptive projections, which are located in the dorsal half of the dorsal column. The crossed corticospinal tract projects in the ventral half of the dorsal columns, unlike humans, where most corticospinal axons are located in the lateral columns. *A–F,* In sections rostral to the contusion site, the spinal cord morphology is still maintained with a clear differentiation of white and gray matter. Note the hypointensity in the dorsal part of the dorsal columns (*arrowheads*) identical to ascending proprioceptive projections. *G–I,* At the lesion center, the spinal cord diameter is reduced and gray and white matter can no longer be separated. Hypointensities located in the center (*G*) reflect hemosiderin deposits. *J–L,* Caudal to the lesion, the gray-white matter contrast is preserved. Both in rostral and caudal scans (*B–D* and *J–L*) hyperintense signals are found in the dorsal columns consistent with cystic defects (see also Fig 3). Hypointensities in axial scans rostral to the lesion correspond to ascending sensory projections, whereas in caudal scans they represent the area of the corticospinal tract (*J–L, arrowheads*).

In Vivo MR Imaging of Contused Spinal Cord

Five animals with spinal cord contusions at thoracic level applied by the IH Impactor and one intact animal were analyzed with MR imaging 2, 6, and 8 weeks postoperatively. Only 2 of 5 injured animals survived the MR imaging procedure and were thus available for histologic evaluation. Most signal intensity changes observed in ex vivo spin-echo images in the contused spinal cord were almost identical to in vivo gradient-echo images of the contused spinal cord. The cord diameter was reduced at the lesion center; in particular, the dorsolateral aspects were atrophic (Figs 4*A–F* and 5*E, -F*), which was confirmed by identical findings in corresponding Nissl-stained histologic sections. Toward the lesion epicenter, the gray/white matter differentiation completely vanished (Fig 5*D–G*). The signal intensity pattern of the gray matter in the intact spinal cord (Fig 1*C, -D*) was replaced by hypointense areas in the center of the cord surrounded by a hyperintense rim dorsally and ventrally (Fig 5*D–G*). As described in ex vivo MR imaging (Fig 2*F, -G*), the hypointensities at the lesion center represent hemosiderin deposits, which are remnants of the hemorrhage caused by the trauma corresponding to dark areas in Nissl- and Prussian-blue–stained sections (Fig 4*K, -N*). In addition, hypointensities were found confined to the dorsal columns rostral and caudal to the lesion, both in sagittal and axial scans (Figs 4*B, -E,* and 5*H*), which are also paralleled by ex vivo MR imaging findings. These hypointensities could be correlated with hemosiderin deposits as depicted by Prussian Blue staining of corresponding spinal cord sections (Fig 4*K*). There was no correlation with areas of macrophage/monocyte infiltration (Fig 4*L–O*), which are—in addition to being located adjacent to the injury center—commonly identified in white matter tracts remote from the lesion site highlighting areas of ongoing Wallerian degeneration (N. Weidner, unpublished observation).

In Nissl-stained histologic sections (Fig 4*H*), small cigar-shaped cystic areas decreasing in size rostrally were identified, which represent areas of beginning post-traumatic syrinx formation. In vivo MR imaging did not produce correspondingly identifiable signal intensities (Fig 4*B, -E*). Most likely, the chosen sagittal imaging planes did not include the location of the central canal.

Discussion

This study was undertaken to evaluate the capabilities of high-field (17.6T) MR imaging to identify morphologic changes occurring after experimental spinal cord contusion injury in adult rats. Findings from this study will serve as a basis for future preclinical experiments employing high-field MR imaging to monitor cell-based regenerative strategies in the injured spinal cord, which might become a relevant therapy for spinal cord–injured human subjects.

To the best of our knowledge, thus far only a few publications have described findings of morphologic changes obtained by MR imaging in vivo in spinal cord–injured rats.[11–19]

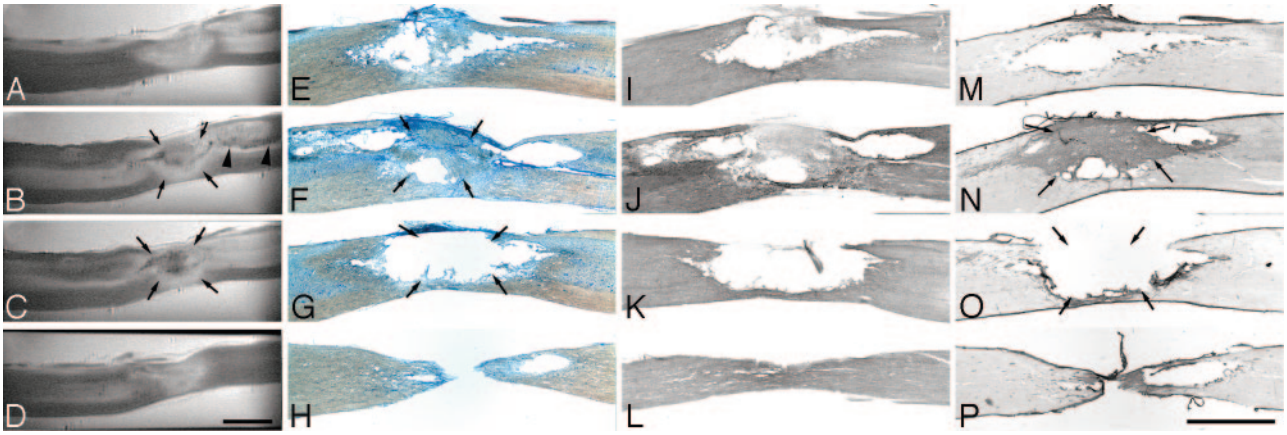

Fig 3. Sagittal ex vivo MR imaging scans of contused rat spinal cord and corresponding histology. Midthoracic contusion injury 4 weeks postlesioning; same specimen as Fig 2 (2D multisection spin-echo; section thickness, 208 μm; FOV, 20 × 6 mm; in-plane resolution, 23 × 78 μm; TE, 7.5 milliseconds; TR, 2 seconds). Scale bar, 2 mm. *A–D,* Ex vivo MR imaging scans from lateral to medial. *E–H,* Corresponding Nissl-stained sections. *I–L,* Corresponding GFAP immunostained sections. *M–P,* Corresponding collagen type III immunostained sections. Homogenous hyperintensities at the injury center (*A*) correspond to cystic lesion defects in histologic sections (*E, I,* and *M*). In other sections. mixed hypo-/hyperintensities in the lesion center (*B* and *C, arrows*) are associated either with cystic lesion defects, hemosiderin deposits, or fibrotic scar formation (*F, N, G,* and *O, arrows*). A hypointensity following the path of the dorsal corticospinal tract caudal to the lesion—corresponding to hypointensities in the dorsal columns in axial MR images (Fig 2)—is highlighted by *arrowheads* (*B*).

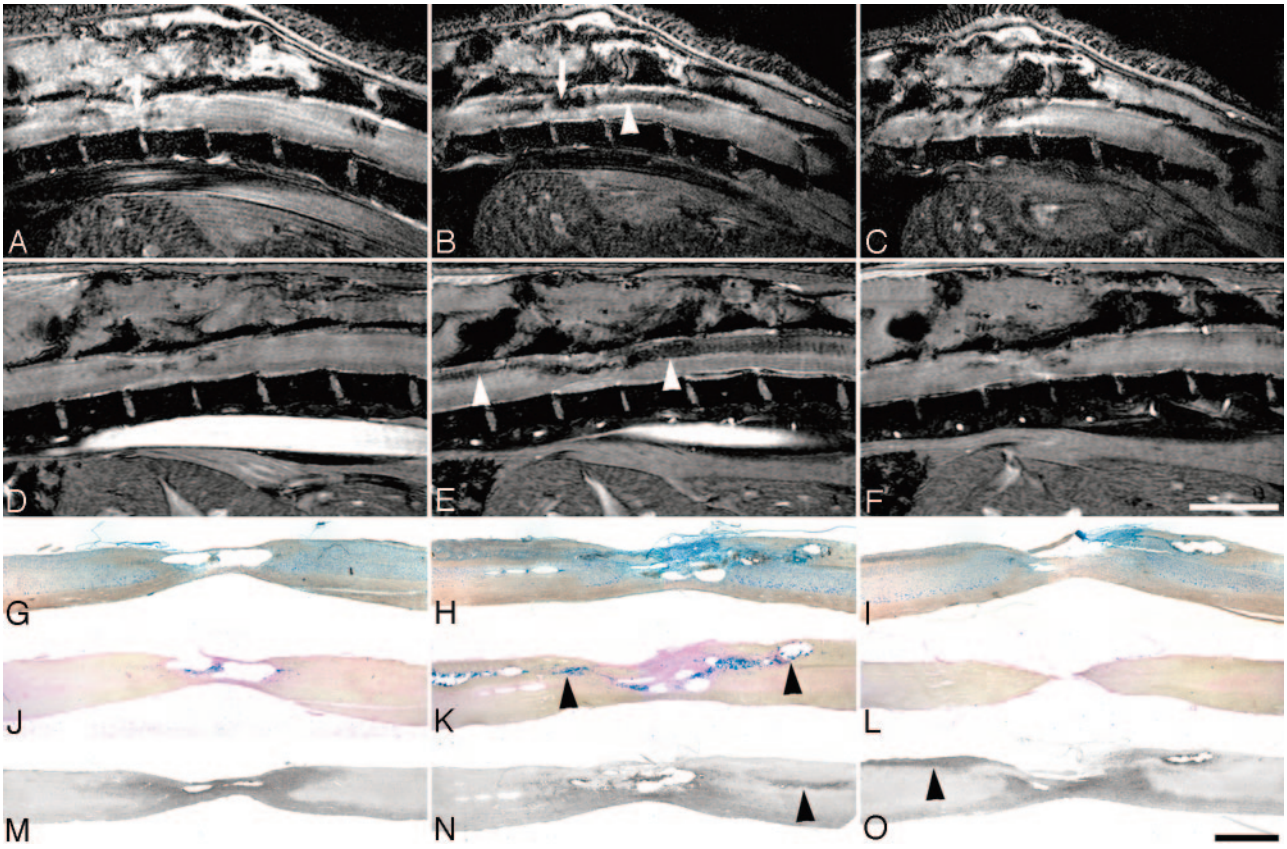

Fig 4. Sagittal in vivo MR imaging scans of contused rat spinal cord and corresponding histology. In vivo MR imaging in adult rats at 2 and 8 weeks after thoracic contusion injury displays signal intensity changes, which parallel the ex vivo MR imaging data (2D multisection gradient-echo; *A–C,* section thickness, 311 μm; FOV, 30 × 30 mm; in-plane resolution, 117 × 117 μm; TE, 4.4 milliseconds; TR, ~200 milliseconds, depending on heart rate; *D–F,* section thickness, 300 μm; FOV, 40 × 25 mm; in-plane resolution, 156 × 98 μm; TE, 3.7 milliseconds; TR, 200 milliseconds, depending on heart rate). Scale bar *A–F,* 5 mm; G–O, 1 mm. Consecutive sagittal MR images are shown at 2 weeks (*A–C*) and 8 weeks (*D–F*) postinjury with corresponding histologic Nissl (*G–I*) and Prussian-blue (*J–L*) –stained sections, and sections processed for ED1 immunohistochemistry (macrophages, monocytes; *M–O*), all from the same animal. *Arrows* in *A* and *B* highlight the site of the impact. Hypointensities along ascending and descending axon projections in the dorsal columns (*B* and *E*) correlate with hemosiderin deposits (*K*) rather than macrophage/monocyte infiltration (*O;* respective areas are indicated by *arrowheads*). These changes increase from 2 weeks (*C*) until 8 weeks (*G*) postinjury. The clear reduction in cord diameter over time (*B* vs *E* and *C* vs *F*) corresponds to the atrophy seen in histologic sections (*G–O*).

Of these, only 2 MR imaging studies investigated spinal cord contusion injuries,[16,18] which are considered to mimic closely pathomorphologic changes occurring after spinal cord injury in human subjects. In all previous studies, only a very limited resolution was achieved at field strengths ranging from 1.5T to 7T. Lower field strengths limit the achievable spatial resolution due to SNR restrictions. Therefore, in-plane resolution and section thickness have to be reduced. The best resolution

Table 2: Comparison of spatial resolutions in previous rat spinal cord injury in vivo MR imaging studies*

Voxel Volume (nl)	In-Plane Resolution (μm)	Section Thickness (μm)	Field Strength	Coil Type	Study
2.25	78 × 78	370	17.6T	Surface coil	Present study
12.2	78 × 156	1000	1.9T	Implanted	Ford et al[11]
304	780 × 780	500	1.5T	Surface coil	Guizar-Sahagun et al[12]
17.3	76 × 76	3000	4.7T	Surface coil	Fraidakis et al[13]
76	195 × 195	2000	2.1T	Surface coil	Fukouka et al[14]
	Information not provided	2800	2T	Surface coil	Ohta et al[15]
80	200 × 200	2000	4.7T	Birdcage coil	Metz et al[16]
12.7	130 × 98	1000	2T	Implanted	Bilgen et al[17]
8.1	78 × 104	1000	7T	Implanted	Narayana et al[18]

*If one study used different resolutions, the highest resolution is quoted.

was achieved with implanted coils,[11,17,18] which improve the SNR compared with surface coils but require an additional surgical procedure. Despite the use of a surface coil, we were able to achieve a spatial resolution at 17.6T, which is 4 times higher than the best previously reported resolution with an implanted coil (Table 2). White and gray matter differentiation,[13,16,17] the delineation of cyst formation, and hemorrhage from surrounding intact spinal cord parenchyma have been reported.[13,17] None of these studies, however, was able to spatially allocate respective signal intensity changes as precise as in the present study. The ability to visualize signal intensity changes at a high spatial resolution will become particularly relevant for future MR imaging studies employed to track the survival and migration of a small number of paramagnetically labeled transplanted cells in the injured spinal cord in small animals.[22]

Both ex vivo and in vivo MR imaging of injured rat spinal cords consistently depicted hypointensities in the dorsal columns rostral and caudal to the contusion injury at the thoracic level. The comparison with corresponding histologic sections revealed that these hypointense areas represent hemosiderin deposits due to trauma-induced hemorrhage. Whether moderate hypointense signal intensity changes as seen with MR imaging ex vivo exactly confined to the area of ascending sensory pathways rostral to the spinal cord lesion represent Wallerian degeneration, which has also been described to induce hypointensities following spinal cord injury,[23] cannot be excluded. Both neuropathologic and the neuroradiologic studies frequently report structural changes representing hemorrhage following spinal trauma.[17,24,25] Respective changes, however, are observed in the gray matter accentuated in and adjacent to the lesion center. To the best of our knowledge, extensive white matter MR imaging signal intensity changes representing hemosiderin deposits as observed in the present study have not yet been described. Field strength–dependent changes in terms of relaxation rates and the higher spatial resolution seem to have increased the contrast in regions of iron deposition,[26] thus allowing visualization of relatively discrete hemosiderin deposits within the spinal cord. Whether the signal intensity changes observed in this animal model of spinal cord injury reflect pathologic sequelae of this disease condition in humans remains to be determined. In case hemosiderin deposits re-

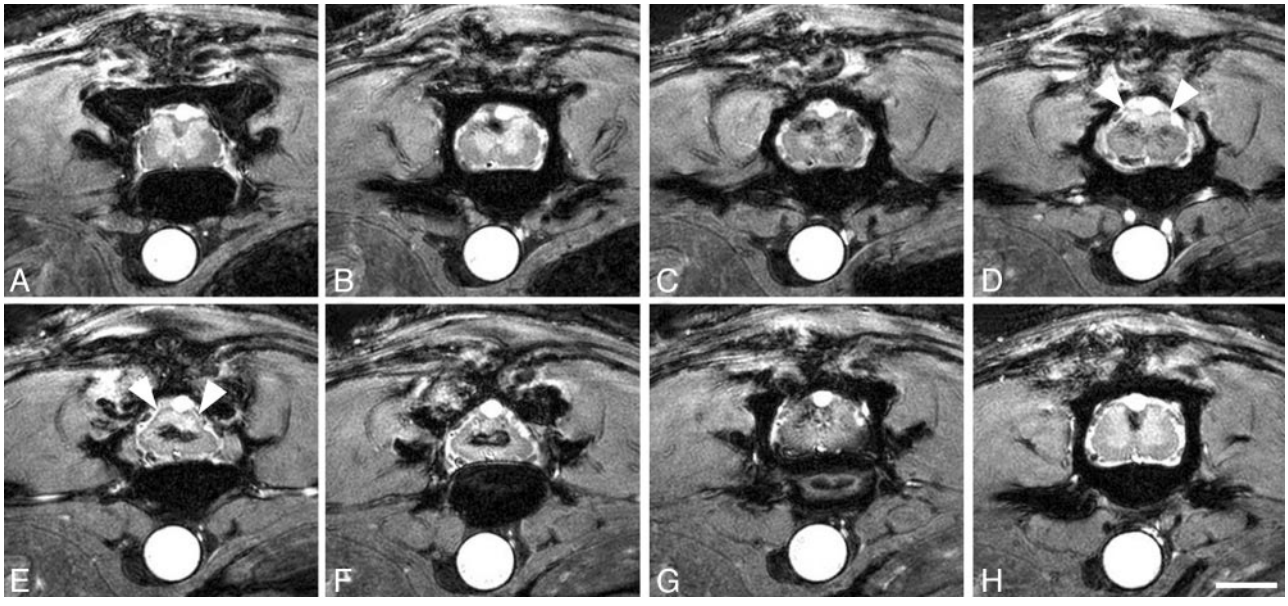

Fig 5. Axial in vivo MR imaging scans of contused rat spinal cord. In vivo MR axial scans in adult rats 6 weeks postinjury (2D multisection gradient-echo; section thickness, 370 μm; FOV, 20 × 20 mm; in-plane resolution, 78 × 78 μm; TE, 4.2 milliseconds; TR, ~200 milliseconds, depending on heart rate). Scale bar, 2 mm. Scans rostral to the contusion (*A–C*), at the lesion center (*D–G*), and caudal to the lesion (*H*). The clear differentiation between white and gray matter disappears over subsequent sections. At the lesion center, hypointensities are surrounded by hyperintensities, which are less pronounced toward the cord surface (*E* and *F*). The dorsal aspect of the spinal cord at the lesion site appears more homogenously hyperintensive, most likely representing cystic changes (*D* and *E, arrowheads*). Signs of atrophy are present in the dorsolateral spinal cord (*E* and *F*).

flecting a former hemorrhage are more widespread than previously thought, free radicals accumulating after an intraspinal hemorrhage might further contribute to the poor intrinsic regenerative capacity of the injured mammalian spinal cord.[27]

Ex vivo and in vivo MR imaging results show a mismatch of MR images and corresponding histologic sections (Nissl stains) in regard to the extent of cystic defects. In histologic sections, we frequently observe a rather large cystic lesion defect upon microscopic analysis, which overestimates the true size of cystic changes. During the preparation of histologic sections from contused spinal cord tissue, nonorganized material such as cell debris, macrophages mixed with remnants of previous hemorrhages filling the cyst in part is lost. In contrast, MR signal intensity changes in corresponding areas are much more diverse, displaying not only hyperintensities reflecting cystic degeneration as suggested by histology but also hypointensities representing hemosiderin and cell debris. Thus, in vivo visualization by MR imaging provides invaluable additional information that cannot be obtained from histologic examination. For example, it is extremely important to differentiate between these alterations in cell transplantation approaches. Transplanting cells in a milieu rich in inflammatory cells and hemosiderin will reduce the survival rate of transplanted cells, thus jeopardizing the transplantation success.[28] Analyzing these changes over time by using MR imaging will help establish the optimal timing and location for transplantation after injury.

A significant limitation for small animal imaging at 17.6T at this point is the reported poor survival rate of rats induced by the scanning procedure. Even though a custom-built probe head was used to overcome spatial restrictions,[21] the tight fitting of experimental animals can sometimes lead to insufficient air circulation, which results in a rise of the isoflurane concentration around the animal. Furthermore, the gradient cooling unit was maintained at 37°C ± 2°C throughout the imaging protocol to control the animals' body temperatures. Because only the temperature of the gradient cooling unit, but not the actual body temperature of the animals, was monitored, it is conceivable that the temperature of the animal was beyond physiologic levels, thus contributing to the observed mortality.

Conclusion

The present study was conducted to investigate the capabilities of high-field MR imaging to monitor structural changes occurring after spinal cord injury in rats. Results demonstrate that MR imaging at 17.6T by using a surface coil provides extremely high-resolution visualization of structural changes occurring in the rat spinal cord following a contusion injury ex vivo and in vivo, which is superior to the best-known spatial resolution even with implantable coils. The achieved spatial resolution allows exact localization of morphologic changes such as cyst formation and hemosiderin deposition, which are sometimes not seen with even histologic analysis of spinal cord–injured animals over time. In principle, in vivo high-resolution MR imaging should allow repeated structural analysis in individual animals, which would also help reduce significantly the number of animals required for preclinical investigations.

Acknowledgments

This study was supported by Deutsche Forschungsgemeinschaft (grant Ha 1232/13). We would like to thank S. Aussenhofer and M. Caioni for expert technical assistance. We also would like to thank V. Herold and E. Rommel for helpful discussions throughout the course of this study and N. Seiberlich for helpful comments on the manuscript.

References

1. Manelfe C. **Imaging of the spine and spinal cord.** *Curr Opin Radiol* 1991;3:5–15
2. Hadley DM, Teasdale GM. **Magnetic resonance imaging of the brain and spine.** *J Neurol* 1988;235:193–206
3. Flanders AE, Spettell CM, Tartaglino LM, et al. **Forecasting motor recovery after cervical spinal cord injury: value of MR imaging.** *Radiology* 1996;201:649–55
4. Grill R, Murai K, Blesch A, et al. **Cellular delivery of neurotrophin-3 promotes corticospinal axonal growth and partial functional recovery after spinal cord injury.** *J Neurosci* 1997;17:5560–72
5. Xu XM, Guenard V, Kleitman N, et al. **Axonal regeneration into Schwann cell-seeded guidance channels grafted into transected adult rat spinal cord.** *J Comp Neurol* 1995;351:145–60
6. Li Y, Field PM, Raisman G. **Repair of adult rat corticospinal tract by transplants of olfactory ensheathing cells.** *Science* 1997;277:2000–02
7. Liu Y, Kim D, Himes BT, et al. **Transplants of fibroblasts genetically modified to express BDNF promote regeneration of adult rat rubrospinal axons and recovery of forelimb function.** *J Neurosci* 1999;19:4370–87
8. Ramon-Cueto A, Cordero MI, Santos-Benito FF, et al. **Functional recovery of paraplegic rats and motor axon regeneration in their spinal cords by olfactory ensheathing glia.** *Neuron* 2000;25:425–35
9. Teng YD, Lavik EB, Qu X, et al. **Functional recovery following traumatic spinal cord injury mediated by a unique polymer scaffold seeded with neural stem cells.** *Proc Natl Acad Sci U S A* 2002;99:3024–29
10. Pfeifer K, Vroemen M, Blesch A, et al. **Adult neural progenitor cells provide a permissive guiding substrate for corticospinal axon growth following spinal cord injury.** *Eur J Neurosci* 2004;20:1695–704
11. Ford JC, Hackney DB, Joseph PM, et al. **A method for in vivo high resolution MRI of rat spinal cord injury.** *Magn Reson Med* 1994;31:218–23
12. Guizar-Sahagun G, Rivera F, Babinski E, et al. **Magnetic resonance imaging of the normal and chronically injured adult rat spinal cord in vivo.** *Neuroradiology* 1994;36:448–52
13. Fraidakis M, Klason T, Cheng H, et al. **High-resolution MRI of intact and transected rat spinal cord.** *Exp Neurol* 1998;153:299–312
14. Fukuoka M, Matsui N, Otsuka T, et al. **Magnetic resonance imaging of experimental subacute spinal cord compression.** *Spine* 1998;23:1540–49
15. Ohta K, Fujimura Y, Nakamura M, et al. **Experimental study on MRI evaluation of the course of cervical spinal cord injury.** *Spinal Cord* 1999;37:580–84
16. Metz GA, Curt A, van de Meent H, et al. **Validation of the weight-drop contusion model in rats: a comparative study of human spinal cord injury.** *J Neurotrauma* 2000;17:1–17
17. Bilgen M, Abbe R, Liu SJ, et al. **Spatial and temporal evolution of hemorrhage in the hyperacute phase of experimental spinal cord injury: in vivo magnetic resonance imaging.** *Magn Reson Med* 2000;43:594–600
18. Narayana PA, Grill RJ, Chacko T, Vang R. **Endogenous recovery of injured spinal cord: longitudinal in vivo magnetic resonance imaging.** *J Neurosci Res* 2004;78:749–59
19. Franconi F, Lemaire L, Marescaux L, et al. **In vivo quantitative microimaging of rat spinal cord at 7T.** *Magn Reson Med* 2000;44:893–98
20. Scheff SW, Rabchevsky AG, Fugaccia I, et al. **Experimental modeling of spinal cord injury: characterization of a force-defined injury device.** *J Neurotrauma* 2003;20:179–93
21. Behr VC, Weber T, Neuberger T, et al. **High-resolution MR imaging of the rat spinal cord in vivo in a wide-bore magnet at 17.6 Tesla.** *Magma* 2004;17:353–58
22. Stroh A, Faber C, Neuberger T, et al. **In vivo detection limits of magnetically labeled embryonic stem cells in the rat brain using high-field (17.6 T) magnetic resonance imaging.** *Neuroimage* 2005;24:635–45
23. Kuhn MJ, Johnson KA, Davis KR. **Wallerian degeneration: evaluation with MR imaging.** *Radiology* 1988;168:199–202
24. Tator CH, Koyanagi I. **Vascular mechanisms in the pathophysiology of human spinal cord injury.** *J Neurosurg* 1997;86:483–92
25. Holtz A, Nystrom B, Gerdin B, et al. **Neuropathological changes and neurological function after spinal cord compression in the rat.** *J Neurotrauma* 1990;7:155–67
26. Schenck JF, Zimmerman EA. **High-field magnetic resonance imaging of brain iron: birth of a biomarker?** *NMR Biomed* 2004;17:433–45
27. Petzold A, Rejdak K, Belli A, et al. **Axonal pathology in subarachnoid and intracerebral hemorrhage.** *J Neurotrauma* 2005;22:407–14
28. Okano H, Ogawa Y, Nakamura M, et al. **Transplantation of neural stem cells into the spinal cord after injury.** *Semin Cell Dev Biol* 2003;14:191–98